



Trends of tropical tropospheric ozone from 20 years of European satellite measurements and perspectives for the Sentinel-5 Precursor

Klaus-Peter Heue¹, Melanie Coldewey-Egbers¹, Andy Delcloo², Christophe Lerot³, Diego Loyola¹, Pieter Valks¹, and Michel van Roozendael³

¹Deutsches Zentrum für Luft- und Raumfahrt, Münchener Str. 20, 82234 Oberpfaffenhofen, Germany

²Royal Meteorological Institute, Avenue Circulaire 3, 1180 Brussels, Belgium

³Royal Belgian Institute for Space Aeronomy, Ringlaan 3, 1180 Brussels, Belgium

Correspondence to: Klaus-Peter Heue (klaus-peter.heue@dlr.de)

Received: 21 April 2016 – Published in Atmos. Meas. Tech. Discuss.: 3 June 2016

Revised: 22 September 2016 – Accepted: 23 September 2016 – Published: 13 October 2016

Abstract. In preparation of the TROPOMI/S5P launch in early 2017, a tropospheric ozone retrieval based on the convective cloud differential method was developed. For intensive tests we applied the algorithm to the total ozone columns and cloud data of the satellite instruments GOME, SCIAMACHY, OMI, GOME-2A and GOME-2B. Thereby a time series of 20 years (1995–2015) of tropospheric column ozone was generated. To have a consistent total ozone data set for all sensors, one common retrieval algorithm, namely GODFITTv3, was applied and the L1 reflectances were also soft calibrated. The total ozone columns and the cloud data were input into the tropospheric ozone retrieval. However, the tropical tropospheric column ozone (TCO) for the individual instruments still showed small differences and, therefore, we harmonised the data set. For this purpose, a multilinear function was fitted to the averaged difference between SCIAMACHY's TCO and those from the other sensors. The original TCO was corrected by the fitted offset. GOME-2B data were corrected relative to the harmonised data from OMI and GOME-2A. The harmonisation leads to a better agreement between the different instruments. Also, a direct comparison of the TCO in the overlapping periods proves that GOME-2A agrees much better with SCIAMACHY after the harmonisation. The improvements for OMI were small.

Based on the harmonised observations, we created a merged data product, containing the TCO from July 1995 to December 2015. A first application of this 20-year record is a trend analysis. The tropical trend is $0.7 \pm 0.12 \text{ DU decade}^{-1}$. Regionally the trends reach up to $1.8 \text{ DU decade}^{-1}$ like on

the African Atlantic coast, while over the western Pacific the tropospheric ozone declined over the last 20 years with up to $0.8 \text{ DU decade}^{-1}$. The tropical tropospheric data record will be extended in the future with the TROPOMI/S5P data, where the TCO is part of the operational products.

1 Introduction

Tropospheric ozone is harmful to humans (Nawrot et al., 2006) and plants. According to Feng and Kobayashi (2009) it is responsible for 5 % crop loss for potatoes and up to 19 % for beans and soybeans. For India, Debaje (2014) estimated a crop loss of 5–11 % for winter wheat and 3–6 % for rabi rice due to ozone exposure. Moreover, in the troposphere, ozone acts a greenhouse gas with a radiative forcing of $0.4 \pm 0.2 \text{ W m}^{-2}$ (Hartmann et al., 2013). This means it ranks third after CO_2 ($1.82 \pm 0.17 \text{ W m}^{-2}$) and CH_4 ($0.48 \pm 0.05 \text{ W m}^{-2}$). Tropospheric ozone is a secondary pollutant that builds up in the atmosphere due to photochemical reactions. The main precursors are NO_x and VOCs which are to a large extent caused by anthropogenic emissions. Ozone plays a key role in the HO_x chemistry and the methane oxidation. The tropospheric lifetime of ozone is of the order of 22 days. More details on the sources, the sinks and the importance of ozone in the atmospheric chemistry can be found elsewhere (e.g. Monks et al., 2015).

Most ozone measurements have been performed close to the surface in the boundary layer. The trends calculated from these time series can not directly be compared to satellite observations but may give a first indication for the trend in the specific region. Summaries of the in situ trends are given in Hartmann et al. (2013), Cooper et al. (2014), Oltmans et al. (2013). Multi-model analysis (Young et al., 2013) suggests that the total ozone burden increased by $\approx 30\%$ since the mid-20th century, indicating that roughly 30 % are caused by anthropogenic emissions of ozone precursors. The first ozone measurements were performed at the end of the 19th century close to Paris, so pre-industrial measurements of ozone do not exist and at least until the 1930s they are highly uncertain (Cooper et al., 2014). Many models have some issues with reconstructing the low ozone levels in Europe in the 1950 and earlier (Parrish et al., 2014). Between the 1950s and the year 2000 the ozone concentrations in Europe had probably doubled (Hartmann et al., 2013). In Europe and the US, ozone reduction efforts were taken and the emissions of many precursors have been reduced in the last 10–20 years. Thereby the typical summertime peak ozone concentrations could be reduced regionally (Cooper et al., 2014). In developing countries ozone concentrations still increase due to the growing emission of ozone precursors. Sun et al. (2016) found an increase in summertime ozone at Mt Tai in central China of $2.1 \pm 0.9 \text{ ppb yr}^{-1}$.

In the tropics the trend varies regionally. Based on in situ measurements in the marine boundary layer (1977–2002) Lelieveld et al. (2004) found an increase of 0.4 ppb yr^{-1} for the northern tropical Atlantic and slightly smaller increases between 0 and 20°S . For the tropical Pacific a positive trend (0.14 ppb yr^{-1}) was found for Hawaii (19.5°N) and insignificant trends are recorded in American Samoa (14°S) (Oltmans et al., 2013).

Based on satellite observations a global access to the trend data is possible; however the earliest observations date back to 1977 (TOMS, Total Ozone Mapping Spectrometer). The global (60°S – 60°N) ozone burden increased by 1.9 Tg yr^{-1} or $0.71 \% \text{ yr}^{-1}$ between 2005 and 2014 (Cooper and Ziemke, 2014). An insignificant decline was found by Ziemke et al. (2005). They studied a combination of TOMS and SAGE ozone data between 1977 and 2003 over the tropical Pacific Ocean. They confirmed their results by extending the time series with OMI data up to 2010 (Ziemke and Chandra, 2012). From SCIAMACHY limb-nadir matching data (2002–2011) Ebojje et. al (2016) retrieved an insignificant positive trend for the tropics in general ($\approx 0.55 \text{ DU decade}^{-1}$), but a significant trend of $\approx 4 \pm 1 \text{ DU decade}^{-1}$ for southern central Africa. According to their data, the tropospheric column ozone decreased on the South American west coast and the neighbouring Pacific with the same order of magnitude. Beig and Singh (2007) used a combination of Nimbus 7 and the TOMS to retrieve a time series of tropospheric column ozone (30°S to 30°N) between 1979 and 2005. According to their trend studies, the tropospheric ozone burden increased by up

to 7 %, especially over South East Asia and is transported westwards to Bay of Bengal and further to the Arabian Peninsular. Furthermore, over central Africa and the southern tropical Atlantic they found a significant positive trend. Over the Pacific Ocean no significant trend is found from the satellite-based tropospheric column ozone (Beig and Singh, 2007).

Fishman and Larsen (1987) were the first to derive tropospheric columns. They subtracted Stratospheric Aerosol and Gas Experiment (SAGE) ozone profile data from TOMS and thereby invented the ozone residual technique to derive tropospheric column ozone. Other approaches to derive the tropospheric column ozone from satellites were developed (e.g. Ziemke et al., 2011; Miles et al., 2015). Many of them rely on the residual technique where the stratospheric column is subtracted from the total column. In the convective cloud differential (CCD) method both the stratospheric and the total column product are derived from the same satellite data. The stratospheric column is estimated based on the ozone column above deep convective clouds, which shield the tropospheric ozone. For cloud-free observation, on the other hand, the troposphere is included in the total column. This method was first applied to TOMS data by Ziemke et al. (1998).

We derived tropical tropospheric column ozone (TCO) using the CCD algorithm (Ziemke et al., 1998; Valks et al., 2014). CCD algorithms rely on total ozone and cloud data; both are taken from GODFITv3 data, available in ESA's Ozone CCI. The average cloud top pressure for deep convective clouds is about 280 hPa ($\approx 10 \text{ km}$). We used a climatology for harmonising the above-cloud column ozone for different cloud altitudes. To reduce the influence of the climatology to a minimum, we calculated the TCO up to 10 km altitude. We combined the time series of tropical tropospheric ozone, from four European satellites: GOME on ERS-2 (Burrows et al., 1999), SCIAMACHY on ENVISAT (Bovensmann et al., 1999), GOME-2 on MetOp-A (GOME-2A, Callie et al., 2000), GOME-2 on MetOp-B (GOME-2B) and the Finnish–Dutch cooperation OMI (Levelt et al., 2006) flying on the AURA satellite. To get a consistent time series, the data were harmonised at two important steps in the retrieval chain. The first harmonisation took place at the beginning, when the reflectances of the instruments were soft calibrated (Lerot et al., 2014), which led to good consistency between the L2 total columns from the individual instruments. Before combining the time series of the tropical tropospheric column ozone a second harmonisation corrected for different trends and biases in the TCO data. The tropical averaged monthly difference between SCIAMACHY data and those of the other instruments were approximated by a multilinear fit. The fitted function was added to the data of the respective satellite. The intermediate total column ozone (TOZ) were not harmonised here. They were harmonised by Coldewey-Egbers et al. (2015). The differences in the TOZ between the sensors might also depend on the cloud fraction, which has not been considered during the harmonisation of the total columns.

For the first 7 years (1995–2002) only GOME data are available, thereafter the number of data increased with the launches of SCIAMACHY (2002), OMI (2004), GOME-2A (2007) and GOME-2B (2013). In 2003 the tape recorder on ERS-2 failed and only a limited number of GOME data are available, so during our retrieval these latter data were ignored. The contact to ENVISAT was lost in April 2012; therefore SCIAMACHY data were no longer received. AURA, MetOp-A and MetOp-B are still in service so in principle today's data can be analysed. The OMI data are analysed until the end of 2015. For the GOME-2 instruments the total ozone column are currently available until the end of 2014. The algorithm described below is part of the operational processor for TROPOMI/S5P data retrieval, the CCD-based tropospheric column ozone will become operational for TROPOMI. After launch the TROPOMI TCO will also be included in this time series.

The first section explains the data retrieval and some adaptations to the satellites used. It starts with a subsection on the underlying ozone column retrieval and introduces the CCD method to retrieve tropospheric columns before it finalises with a small section on the results and the uncertainties. Before discussing long-term trends we have to make sure that the different sensors measure comparable tropospheric column ozone. Therefore, the data are harmonised and compared to ozone sondes. The paper concludes with the discussion of the TCO trends including comparisons with previous trend studies.

2 Data retrieval

The tropical tropospheric column ozone were retrieved with the convective cloud differential (CCD) method. It was originally invented by Ziemke et al. (1998) and further improved by Valks et al. (2003, 2014). The CCD method retrieves the tropospheric column as the difference between total column ozone and the stratospheric column ozone (SCO). It utilises the processed total ozone columns and cloud data (level 2 data, Sect. 2.1) as retrieval input.

2.1 GODFIT total ozone retrieval

A detailed description of the GODFITv3 algorithm is given in van Roozendael et al. (2012) or Lerot et al. (2014), here it is shortly summarised. The total ozone column data were generated in the framework of the ESA Ozone Climate Change Initiative (Ozone CCI) and are available on the CCI web page: <http://www.esa-ozone-cci.org> (March 2016).

The GODFIT algorithm minimises the difference between a sun-normalised calculated earthshine spectrum and the observation between 325 and 335 nm using standard minimisation tools. Therefore, a linearised forward model is used with the state vector including the TOZ, a temperature shift, the effective surface albedo (polynomial 3rd order),

the Ring-effect correction term and an earthshine Doppler shift. Among other variables, the fit varies the TOZ which is then used to derive an ozone profile from a column classified ozone climatology (Bhartia, 2003) based on TOMS data. For the lowest altitude layers, a better representation was found by replacing the TOMS data with the OMI/MLS tropospheric ozone climatology (Ziemke et al., 2011). Based on the ozone profile as well as the other atmospheric parameters (e.g. temperature profile), the radiative transfer model (LIDORT) calculates the intensity at the top of atmosphere as well as the Jacobian. During each minimisation step the intensity has to be calculated.

The cloud fraction and cloud height are taken from cloud products calculated before from the same instruments. In the effective scene approach as proposed by Coldewey-Egbers et al. (2005), the effective altitude results from the cloud fraction weighted mean of the cloud top height and the ground altitude. The effective surface albedo is included in the GODFIT minimisation retrieval. Even though the retrieval only includes the column above the effective surface, the total column still represents the complete column including the troposphere. The final profile is integrated between the surface and the cloud altitude to calculate the ozone column below and inside the cloud (ghost column).

For GOME, SCIAMACHY, GOME-2A and GOME-2B the cloud data (altitude and cloud fraction) are taken from the FRESCO v6 algorithm (Wang et al., 2008), which is based on the O₂ A-band. Due to the shorter spectral range the OMI cloud data are derived from O₂–O₂ absorptions at 477 nm. The cloud albedo is fixed at 0.8 in both cloud algorithms. For S5P the cloud data will be calculated using the OCRA/ROCINN algorithm, which is also based on the O₂ A-band (Schuessler et al., 2014; Loyola et al., 2010). The TROPOMI offline total ozone data product will be retrieved with the GODFIT algorithm.

Although the same algorithm was applied to GOME, SCIAMACHY and GOME-2A including the cloud algorithm, the total ozone columns of the three sensors deviated from each other and possibly showed temporal drifts (Fig. 7 in Lerot et al., 2014). Instrumental degradation (e.g. Coldewey-Egbers et al., 2008) causes errors in the absolute radiation of the level 1 data, thereby causing errors in the TOZ and the effective albedo retrieval. As a solution, a soft calibration of the data was introduced. The measured spectra are compared to simulated spectra in the wavelength range between 325 and 335 nm. The simulated spectrum depends on the ozone column; therefore for eight European stations Brewer ozone columns were included in the simulation of the respective spectra. Look-up tables of reflectance corrections factors for the different sensors were built, which depend on the wavelength, the time, the solar zenith angle and the instrument viewing angle. The measured reflectance is multiplied with the correction factor, properly interpolated through the look-up table.

A direct consequence of this soft calibration is to somehow align the retrieved ozone columns to the Brewer observations. In future versions a new calibration method based only on satellite observations is planned for the harmonisation of the total ozone columns.

To filter out outliers, the total column data are rejected if the rms fit residuals exceed an instrument-dependent threshold. In total roughly 2 % of the data were rejected.

2.2 Convective cloud differential method for TROPOMI

The tropospheric column ozone will be operationally calculated from both the near real time and the offline total ozone columns for TROPOMI. The convective cloud differential algorithm summarised in the following originates from Valks et al. (2014). Compared to the original algorithm some improvements and adaptions to the GODFIT data have been made. The tropospheric columns can only be measured by satellites during cloud-free observations. On the other hand this means that observations above high-reaching clouds hardly contain any tropospheric signal. Therefore, the measurements above deep convective clouds with a large cloud cover can be used to estimate the stratospheric column. For the retrieval of the total column (Sect. 2.1), this effect is considered by adding a ghost column to the stratospheric signal. The ghost column is based on a climatology and includes the lowest part of the column, below as well as inside the cloud up to the effective cloud top height. Hence subtracting the ghost column from the total column results in the above-cloud columnar ozone (ACCO):

$$\text{ACCO} = \text{TOZ} - \text{ghost}. \quad (1)$$

Compared to Valks et al. (2014) (Eq. 3 therein) this is one adaption to the GODFIT data set and will also be used for offline tropospheric column ozone from TROPOMI.

To determine the stratospheric ozone only, clouds with a top height higher than 8.5 km are taken into account. Nevertheless the cloud top varies in a range from 8.5 km up to ≈ 15 km. The average cloud top height above 8.5 km in the current GODFIT data set is close to 10 km; therefore the ACCO are normalised to 10 km (≈ 280 hPa). For low cloud altitudes, the ACCO includes the partial ozone column between cloud top height and the 10 km level. This partial column is rated by a climatology-based column and subtracted prior to averaging all ACCO observations in a grid cell (Fig. 1). For clouds with a cloud top height above this altitude level, a respective climatology-based correction column is added. For the ozone climatology, we used the sonde-based data set by McPeters et al. (2007). The pressure altitude grid was interpolated to an altitude grid using the climatology from Fortuin and Kelder (1998). The correcting column is typically less than 1 DU. For GOME-2A (Sect. 2.3) and January 2012 we checked the correction column in detail and found an average of -0.006 ± 0.196 DU, the extreme val-

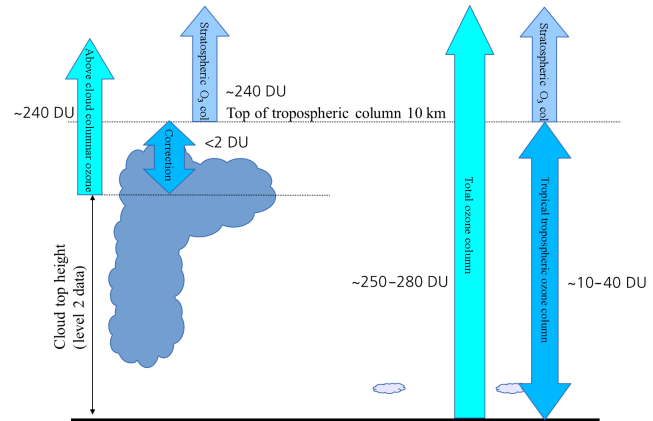


Figure 1. Sketch of the CCD method. The left side illustrates the estimate of the SCO using large convective clouds. In this case the cloud top is below 10 km, hence the correction column is subtracted. On the right the cloud-free measurements of the total column and the TCO are shown.

ues were -2.626 and 7.314 DU. The cloud top altitudes are taken from the cloud data retrieved in a separate step before the ozone retrieval. The cloud top determination is based on either O_2 or O_4 absorptions (Sect. 2.1) and results in an altitude that is typically lower than the physical cloud top level. This causes an uncertainty in the ACCO, partly because the ozone inside the cloud is included in the ACCO (Ziemke et al., 2009).

The top height of 10 km is low for a tropospheric product, but shifting this altitude to higher levels only adds an offset which is given by the climatology profile between the higher altitude and the average cloud top height. Even though the tropical stratosphere begins at roughly 17 km (≤ 100 hPa) we call the corrected ACCO stratospheric column ozone (SCO). The optimal top height for TROPOMI is currently under investigation but can hardly be fixed prior to the launch.

The SCO is determined over a clean reference area with a sufficient frequency of high convective clouds (70° E and 170° W Valks et al., 2014) and averaged over a certain period. In this reference area, the error introduced due to in-cloud ozone is low. For TROPOMI a temporal resolution of several days (≈ 6) might be achieved. Thereby we assume that the stratospheric column ozone is constant in time and longitude. These assumptions are fulfilled in the tropics (Ziemke et al., 2009), which limits the algorithm to a range of 20° S to 20° N. Due to the seasonal migration of the ITCZ the data are binned to latitude bands of 1.25° each.

A measurement pixel is called cloud free if the cloud cover is less than 10 %. The CCD method is sketched in Fig. 1. Here the cloud-free observations as well as the convective cloud measurements are shown simultaneously. On the left, the ACCO is shown as the ozone column above the effective cloud top height given by the cloud retrieval. The correction term between the cloud top height and the fixed level (10 km)

is subtracted from the ACCO. The other part of the figure shows the cloud-free case with less than 10 % cloud fraction, the TCO is the difference between the TOZ and the SCO:

$$\text{TCO} = \text{TOZ}_{\text{cloudfree}} - \text{SCO}. \quad (2)$$

The TCO and TOZs for cloud-free pixels were averaged over the time period used for the SCO and regridded to $2.5^\circ \times 1.25^\circ$ resolution. Negative values in the averaged TCO were skipped. Due to the high resolution of the TROPOMI instrument and the expected large number of data points per grid cell, we assume that the complete ground pixel is in the same grid box as the centre point.

One of the basic assumptions of the CCD method is that the stratospheric column ozone is constant along the latitude bands and for the respective time period. In the winter months this assumption is not always fulfilled on both hemispheres. Stratospheric intrusions cause local changes in the stratospheric columns, which sometimes result in misleading tropospheric column ozone. Usually an automated quality control prevents this consequence for the TCO. The stratospheric reference data must meet four conditions of the quality control to be accepted.

- The stratospheric column must not be lower than 200 DU.
- The number of observations in the stratospheric reference must be higher than a minimum threshold.
- The standard deviation in the stratospheric reference for the certain latitude band must be lower than a certain threshold.
- The gradient in the stratospheric reference must not exceed a certain maximum value ($\approx 5 \text{ DU band}^{-1}$).

The thresholds depend on the instruments and will be adapted to the real measurements as soon as they are available. Currently, default values are used based on the experiences gained in the data retrievals for the instruments mentioned below (Sect. 2.3). In the final algorithm, the time resolution also has to be considered. The standard deviation of the TCO from the individual observations within a grid cell represents both the atmospheric inhomogeneity and the statistical error of the TCO. Therefore, it is an appropriate estimate of the error. The uncertainty in the TCO from TROPOMI can be estimated based on the current instruments (Sect. 2.3) to a range of ≈ 3 to 5 DU. The uncertainty does not depend on the pixel size of the individual observers.

2.3 Adaption of the algorithm to current instruments

The algorithm as described in the previous section (Sect. 2.2) was developed for the TROPOMI instrument on S5P. However, the launch is scheduled for early 2017; therefore the algorithm was applied to the data of the current European satellites: GOME, SCIAMACHY, OMI, GOME-2A and GOME-2B. All these instruments have a coarser resolution and less

coverage. To some extent the algorithm had to be adapted to the different instruments. In a first step we reduced the temporal resolution from ≈ 6 days to 1 month, which increases the number of data points per grid cell. On the other hand the assumption of a temporal stable stratospheric column ozone might not be valid if the sampling period is longer than 1 month.

In the tropics, a grid cell of 2.5° longitude measures less than 280 km, hence it is smaller than a GOME pixel (≈ 320 km). In the latitudinal direction, however, the pixels are by far smaller than the grid cells (≈ 40 km vs. 139 km). Because of that, during the gridding process, the GOME data are weighted with the longitudinal fraction inside a grid box. The OMI footprint is $13 \text{ km} \times 24 \text{ km}$ and hence small enough to apply the original S5P algorithm without any weighting. The TCO differ by $\approx \pm 0.3$ DU between the weighted and the non-weighted averaging even for GOME-2A and SCIAMACHY. The small difference supports the application of the faster and easier operational averaging, also for SCIAMACHY, GOME-2A and GOME-2B. Because for the stratosphere the column between 70° E and 170° W (120° or more than 13 000 km) is averaged, the weighting is not useful at this point for any of the instruments.

It is obvious that the threshold for the number of observations per latitude band differs between OMI and GOME. Also the number of tropospheric columns per grid cell varies between the individual sensors, for OMI the maximum numbers are above 1000 and for GOME the maximum sum of weights is usually between 40 and 60.

The standard deviation of the TCO is log-normal distributed with mean values between 3.3 and 4.39 DU, depending on the instrument. The width varies between 1.33 and 1.77 DU. In the merged product (Sect. 3) the propagated standard deviations of the individual sensors determine the final error to 3.8 ± 1.6 DU.

The algorithm was verified in the framework of the TROPOMI/S5P product development by a similar product from the University of Bremen (Leventidou et al., 2016). When applied to the same total ozone and cloud data, the difference between the two algorithms was typically less than 1 DU. A detailed error discussion based on the error propagation from the fits can be found in Leventidou et al. (2016). While they apply the CCD retrieval to WFDOAS ozone columns, our data are derived from the GODFITv3 total columns (Sect. 2.1). Moreover the spatial resolution is 4 times coarser $5^\circ \times 2.5^\circ$ compared to $2.5^\circ \times 1.25^\circ$. Due to these differences the total error is underestimated compared to our variability based uncertainty: 1 to 2 DU compared to $\approx 3.8 \pm 1.6$ DU.

2.4 CCD results

The first results from TROPOMI are awaited at the beginning of 2017; until then we focus on the existing instruments. The TCO above the tropical Atlantic is strongly influenced by the

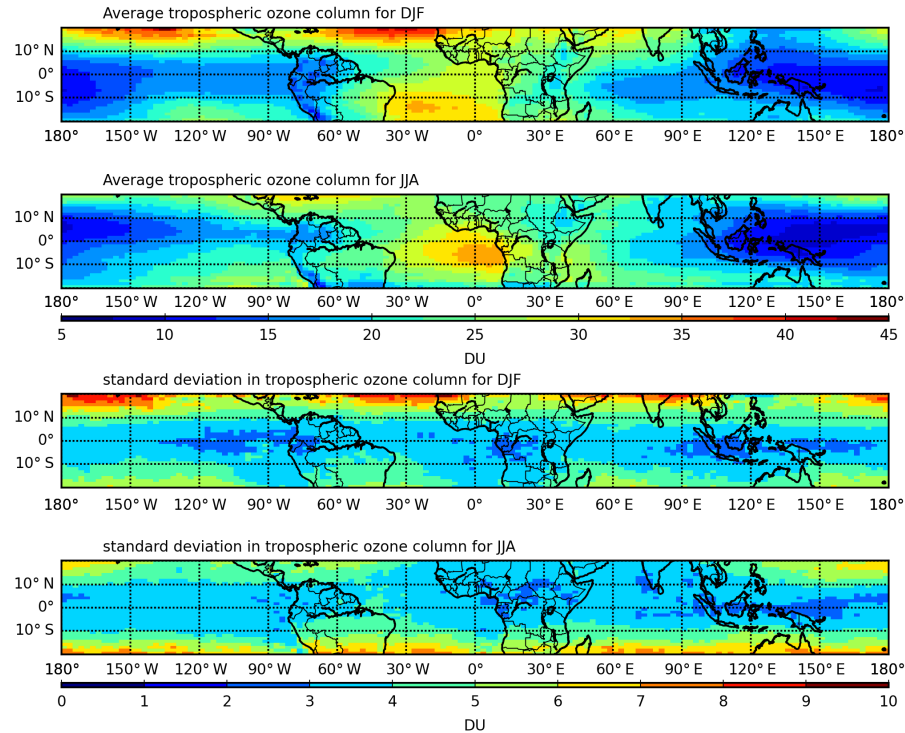


Figure 2. Top: mean tropospheric column ozone for December–February and June–August based on the merged CCD data set from all sensors for 1995 to 2015 (Sect. 3). Bottom: standard deviation of the tropospheric column ozone. Note the different colour bars for the TCO and its deviation.

sources of ozone precursors which originate from the forest fires in central Africa and are transported westwards with the trade winds. The migration of the ITCZ over the African continent causes similar seasonality of the rain season and the burning season, when harvested fields or parts of the rainforests are burned. A respective change in the location of the ozone maximum is visible in Fig. 2. The figure shows the 20-year average tropospheric ozone distribution for December, January, February (DJF) and June, July, August (JJA) as well as the propagated standard deviations from the monthly data. In JJA a clear ozone maximum on the central African coast is observed, in DJF when the burning season is further north, only moderated enhancement is observed there. A stronger maximum is found close to the South American coast and further south. This is probably caused by the biomass burning emissions from South America. Over the central Pacific (150° W to 150° E) the TCO reaches its minimum of less than 10 DU. In the same region, the standard deviation is also low.

The observed standard deviations are enhanced towards the northern edge in the boreal winter and southern edge in the austral winter. This effect is visible in both the merged data and in the data of the individual sensors. It might be related to some dynamical effects e.g. migration of the subtropical jet and the related stratosphere troposphere exchange (e.g. Sprenger et al., 2003). An enhanced downward trans-

port of stratospheric ozone into the troposphere also causes a higher variability in the monthly means. Some of the TCO data at the winter edge of the tropics are dismissed and less data are considered in the averages and the deviations in Fig. 2. The latter indirectly contributes to the higher standard deviation in the winter compared to the summer.

3 Harmonisation

The tropospheric column ozone are harmonised to reduce instrumental effects in the long-term time series. Thereby the different offsets and drifts of the instruments shall be reduced. We used SCIAMACHY as reference and compared the TCO from the other instruments to this reference. SCIAMACHY has a good temporal overlap with OMI, GOME-2A and GOME. Moreover the cloud data are based on the same algorithm as for GOME, GOME-2A and GOME-2B. The longitudinal and latitudinal averaged differences ($\langle \Delta \rangle_{\text{lat,long}}$) of the TCO between the other sensor ("inst" in Eq. 3) and the reference was approximated by a combination of a linear function and several sine and cosine functions with three different periods (1 year, 6 months and 4 months):

$$\begin{aligned} \langle \Delta \rangle(t) &= \langle TCO_{\text{inst}} - TCO_{\text{SCIAMACHY}} \rangle_{(\text{lat}, \text{long})}(t) \\ &= r(t) + a + b \cdot t + \sum_{i=1}^3 (c_i \cdot \sin(\omega_i \cdot t) + d_i \cdot \cos(\omega_i \cdot t)) \\ &= r(t) + \text{cor}_{\text{inst}}(t) \end{aligned} \quad (3)$$

with

$$\omega_i = \frac{2 \cdot \pi \cdot i}{12}, \quad (4)$$

where t is the time in month between January 1995 and December 2015, a , b , c_i and d_i are the fit parameters and $r(t)$ is the residual structure. The difference between the other instrument and SCIAMACHY is averaged over the complete tropics, so the fit parameters do not depend on latitude or longitude but on the instrument. Wherever the fit coefficients were not robust ($> 2 \times \sigma$) they were set to zero. The respective correction function $\text{cor}(t)$ was added to the $TCO(\text{lat}, \text{long}, t)$ for the complete tropics:

$$\begin{aligned} TCO_{\text{inst}}^{\text{harm.}}(\text{lat}, \text{long}, t) &= \\ TCO_{\text{inst}}(\text{lat}, \text{long}, t) + \text{cor}_{\text{inst}}(t). \end{aligned} \quad (5)$$

This means that the difference between the original data set and the harmonised data set depends on the time only. The extrapolation of the correction for the GOME data from 2002 to 2011 back to 1995 was too uncertain. Especially because the largest part of the time overlap between SCIAMACHY and GOME (2002–2011) is affected by the tape recorder failure of GOME. Therefore, many GOME data in this period are at the northern edge of the tropics ($15\text{--}20^\circ \text{N}$), where the data retrieval is often uncertain (Sect. 2.4). As a consequence of that, the number of common data points per month is low. If the data after 2003 are skipped, the overlapping period encompasses just 1 year of data (12 data points), which is not sufficient to fit any trend or even constant function. The GOME data are not harmonised to SCIAMACHY.

For OMI the fit for the offset and the slope (a and b in Eq. 3) were not robust; therefore we replaced the linear part of the harmonisation function (Fig. 3) by the averaged differences. While for GOME and OMI no trend was found or allowed, the difference between SCIAMACHY and GOME-2A showed a strong increase in time $3.3 \pm 0.04 \text{ DU decade}^{-1}$. The reason for this trend is not yet fully understood. If a similar approach is applied to the stratospheric reference column, then the trend of the GOME-2A SCO is $-1.09 \pm 1.2 \text{ DU decade}^{-1}$ relative to SCIAMACHY's SCO. The total columns agree well after the soft calibration is applied. However, in our data set only the cloud-free observations are considered whereas Lerot et al. (2014) took all data into account. MetOp-B was launched into space in September 2012, roughly half a year after the last SCIAMACHY data were received. So the GOME-2B data can not be harmonised to

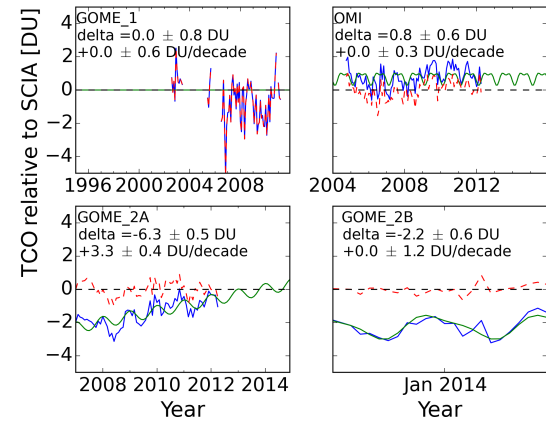


Figure 3. Average difference between the reference (SCIAMACHY) and the other sensors (blue), the fitted functions (cor(t)) in green and the difference to the harmonised data in red (r(t)).

Table 1. Parameters of Gaussian fits to the difference between the other instruments and the reference (SCIAMACHY). For GOME no correction was applied, hence only one set of parameters is listed.

	Bias	Width	Number
GOME	0.46	3.23	27 784
OMI	0.79	2.69	326 893
OMI (harmonised)	0.03	2.68	326 893
GOME-2A	-1.43	2.62	232 911
GOME-2A (harmonised)	0.00	2.55	232 911
GOME-2B	-2.25	2.11	95 113
GOME-2B (harmonised)	0.00	2.05	95 113

SCIAMACHY directly. Therefore, the harmonised GOME-2A and OMI act as reference for GOME-2B.

In the overlapping periods the harmonised TCO agree very well with each other (Table 1). The difference for all TCO between the reference instrument SCIAMACHY and the other observers shows a small Gaussian distribution. The parameters do not change for GOME because here no correction was added. The fit improves slightly for OMI, the bias between GOME-2A and SCIAMACHY is especially reduced.

The maximum differences given in Table 1 or in Fig. 3 reach up to 2 DU. Relative to the tropospheric column ozone of roughly 20 to 40 DU the difference is 10 to 5 %. In the time series of the TCO the differences can be seen (Fig. 4). While in the original data set the OMI TCO is always above the SCIAMACHY data and GOME-2A is mostly below, the harmonised data agree better for all sensors. The observed difference between OMI and SCIAMACHY might also result from real atmospheric changes. The overpass times of the two satellites differ by more than 3 h (10:00 to 13:30 LT). During this time of the day, the tropospheric ozone burden usually increases. For the trend analysis and similar applications it has to be corrected for. On the other hand, the harmonised data must not be used to study diurnal variations.

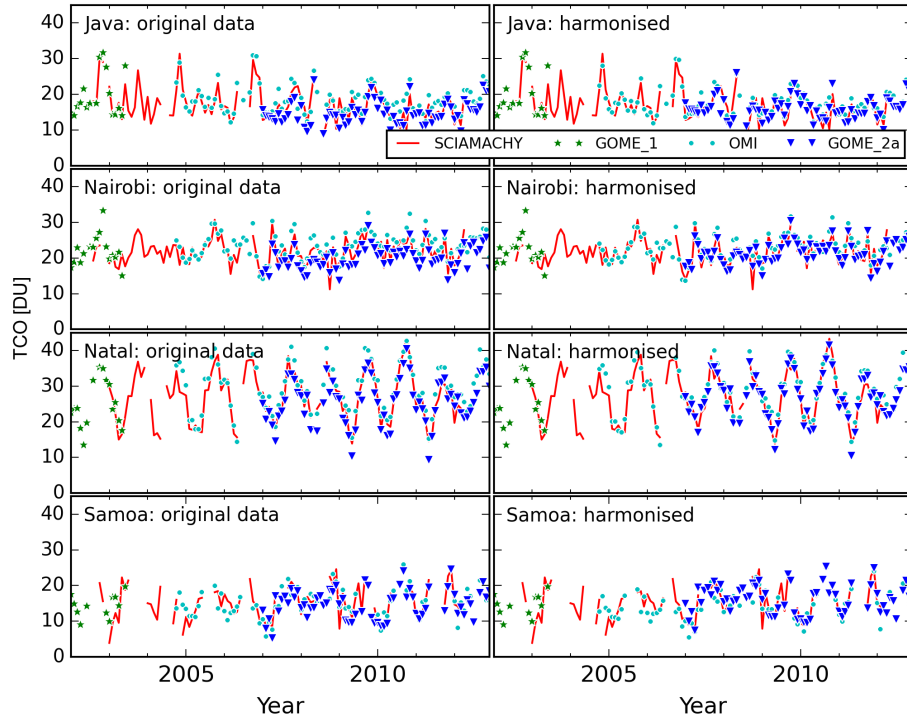


Figure 4. Time series of TCO from SCIAMACHY as well as GOME, OMI and GOME-2A for SCIAMACHY lifetime at four selected sounding stations. Both the OMI and the GOME-2A data clearly deviate from the SCIAMACHY data in the original data (left), the deviation is reduced in the harmonised data (right).

We averaged the harmonised data of the different instruments to a merged data product. For the first 7 years this product is identical to the GOME data. After July 2003, the GOME data are no longer considered in the merged data product as well as in the trend analysis below (Sect. 4).

3.1 Comparison to sondes

After the harmonisation we compared our results with integrated soundings from SHADOZ project (Thompson et al., 2003) and the WOUDC project (<http://www.woudc.org/>, March 2016).

The sonde data from the stations listed in Table 2 were integrated up to 280 hPa (≈ 10 km) according to

$$\text{TCO} = k \cdot \sum (c_i(\text{O}_3) \cdot \delta P_i), \quad (6)$$

where $k = 0.789 \text{ DU ppm}^{-1} \text{ hPa}^{-1}$, P is the pressure in hPa and c is the average ozone mixing ratio at the respective pressure level (<http://www.temis.nl/data/fortuin.html>, February 2016).

The TCO data retrieved in the standard product have a monthly resolution. For most tropical stations four or fewer soundings per month are available. Saunois et al. (2012), however, showed that at least 12 soundings per month are required to adequately represent the monthly mean tropospheric column. Hence we extracted a 3-day product for the

respective sounding days. Especially for GOME, the restriction on the exact soundings days was too strong and hardly any collocated TCO were found. Because of that we calculated a 3-day mean centred around the sounding day and area of $5^\circ \times 5^\circ$ around the sonde station for the validation. The CCD method postulates the stratospheric column to be constant for roughly a month and zonally invariant, hence the monthly stratospheric columns were subtracted from the cloud-free total columns for the specific days and region. In total we have 4688 collocated observations. We added the same correction functions as for the harmonisation (Sect. 3) to the 3-day means for the individual sensors before averaging to the merged data for each sounding station. The difference between the integrated sondes data and the merged satellite-based TCO shows a normal distribution with a mean of -1.7 DU and a width of 5.8 DU , indicating that the satellite data overestimate the TCO compared to the sondes. The top height uncertainty and the in-cloud correction (Sect. 2.2) might be reasons for the observed bias.

The spatial and temporal averaged deviation was further investigated. For the four seasons the mean and the 10th and 90th percentiles are plotted in Fig. 5 for running 5-year periods. At the stations with 4 soundings per month this sampling period of 3 months and 5 years encompasses up to 60 soundings. For Nairobi, it was on average 46 soundings for the period 1995 to 2015. Within the 10th to 90th percentiles

Table 2. SHADOZ and WOUDC stations used for the comparison with the satellite-retrieved tropospheric columns. The first and last sondes included in the comparison are also listed, for 2015 only data from five stations are available. Two of the stations at the end of the table, are too close to the edges of the tropics; therefore they were not considered in the general comparison. The Indian sondes in Poona and Thiruvananthapuram were skipped because we were not sure about the data quality. However, they are mentioned for completeness.

Station	Longitude	Latitude	First sonde	Last sonde
Java	111	-7.6	7 Jan 1998	30 Oct 2013
Singapore	103.8	1.3	18 Jan 2012	20 Aug 2014
Kuala Lumpur	101	2	15 Jan 1998	22 Dec 2014
Nairobi	36.8	-1.3	4 Dec 1996	16 Dec 2015
Ascension Island	-14.4	-8	31 Jul 1997	24 Aug 2010
Natal	-35.4	-5.4	5 Jan 1998	24 Sep 2015
Paramaribo	-55.2	5.8	2 Sep 1999	29 Dec 2014
Costa Rica	-84	10.01	8 Jul 2005	18 Dec 2015
San Cristobal	-89.6	0.9	25 Mar 1998	30 Jan 2014
Papeete	-149.2	-18	31 Jul 1995	27 Dec 1999
Pago Pago (am. Samoa)	-170.6	-14.4	8 Aug 1995	16 Dec 2015
Fiji	178.4	-18.1	26 Feb 1997	30 Oct 2013
Hawaii	-155.04	19.4	4 Jan 1995	25 Feb 2015
Hanoi	105.8	21		
La Réunion	55.48	-21		
Poona	73.8	18.5		
Thiruvananthapuram	76.95	8.5		

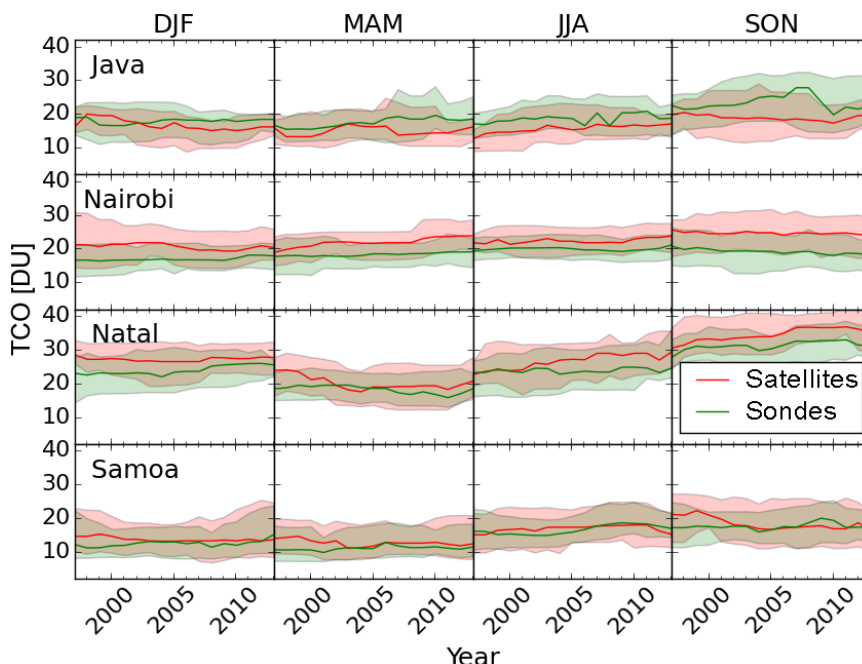


Figure 5. Average TCO for seasonal 5-year sampling. On the *x* axis the interval 1995 to 2000 is shown as 1997. The shaded area illustrates the 10th to 90th percentile interval. For most cases the satellite data (red) and sonde data (green) agree within this range.

margin the data agree quite well. For the stations Nairobi and Natal the merged multi-sensor TCO tends to be higher than the integrated sounding data, as was already mentioned for the histograms.

Despite the algorithm for S5P, the focus of the manuscript is on the trend in tropospheric ozone data based on existing instruments. For example, for Natal a slight trend can be seen in Fig. 5, in JJA and SON. Furthermore, the sonde data seem to follow this trend, especially within the 10th to

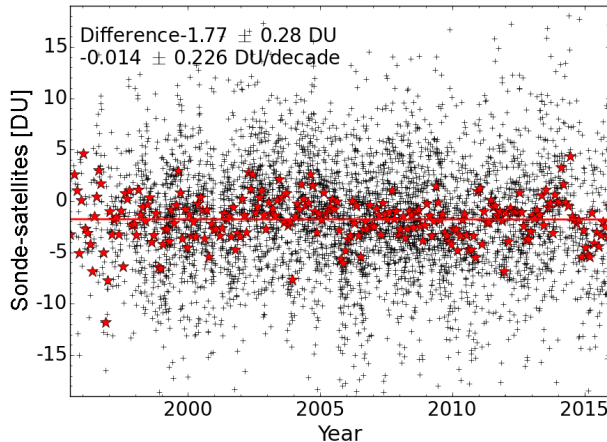


Figure 6. Differences between sondes and the merged data product. The black crosses indicate the difference between the individual sounding and the collocated satellite observation, the red asterisks show the respective monthly mean and the line shows the fit result.

90th percentile range (green band). A drift in the satellites' TCO might be misinterpreted as trend. So for each station in the tropics we subtracted the satellite TCO from the collocated sounding and fitted the combination of linear function and sine and cosine function as in Eq. (3). We used the monthly mean differences as input to the fitting algorithm, rather than the complete data set of the differences. This increased the weight of the beginning and the end of the period where less collocated data are available. For the complete period the merged data product shows only a very small trend compared to the sondes with $-0.014 \pm 0.226 \text{ DU decade}^{-1}$. Compared to the fit error it is negligible and will, therefore, no longer be considered in the trend analysis (Fig. 6). The intercept of the fitted line equals -1.77 DU , hence the bias is confirmed. Also for the individual data points the slope was smaller than the fit error $-0.151 \pm 0.169 \text{ DU decade}^{-1}$.

4 Tropical tropospheric ozone trends

After the harmonisation, we note that the data obtained from the different instruments agree well with each other and with the ozone sondes, and the effects of different temporal drifts are minimised. This is an important requirement for the calculation of long-term trends. For the following trend analysis, we used the merged data set and calculated a tropical trend as well as local trends. To reduce the noise in the local trends, the data were regridded to a $5^\circ \times 5^\circ$ grid. The fitting function consists of the same combination of a linear term, three sine and cosine functions as in Eqs. (3) and (4) and in addition the indices for the quasi-biennial oscillation, for the El Niño and for the solar activity were included. The indices can be found here: QBO for 30 and 50 hPa, <http://www.esrl.noaa.gov/psd/data/correlation/qbo.data>, (January 2016), ENSO http://www.esrl.noaa.gov/psd/gcos_wgsp/Timeseries/

Nino34/, (January 2016) and the 10.7 cm Solar Flux Data are provided as a service by the National Research Council of Canada, <http://www.spaceweather.ca/solarflux/sx-5-mavg-en.php>, (February 2016). The indices data were smoothed with a 3-month running average for ENSO and QBO and a 7-month running average for the solar activity.

$$\begin{aligned} \text{TCO} = & a + b \cdot t + \sum_{i=1}^3 (c_i \cdot \sin(\omega_i \cdot t) + d_i \cdot \cos(\omega_i \cdot t)) \\ & + e \cdot \text{ENSO}_{3.4} + f \cdot \text{solar} + g_{50} \cdot \text{QBO}_{50} + g_{30} \cdot \text{QBO}_{30} \end{aligned} \quad (7)$$

The coefficients a to g depend on latitude and longitude. For the tropical average the same fit was applied as for the individual grid cells. For most grid cells the QBO and the solar indexes turned out to be insignificant. The tropically averaged ozone increases by $0.7 \pm 0.12 \text{ DU decade}^{-1}$ (Fig. 7). Relative to an average TCO of 20 DU it means an increase of $3.5\% \text{ decade}^{-1}$.

Locally the trends vary between -0.8 and $1.8 \text{ DU decade}^{-1}$. Figure 8 shows the fit for the case of the maximum trend (b in Eq. 7). The data were observed on the African coast, in this region influence of El Niño on the TCO is low.

The time series has a very pronounced annual cycle, with a peak to peak amplitude of about 10 DU. The maximum in July/August coincides with maximum fire activity in southern central Africa (e.g. <https://firms.modaps.eosdis.nasa.gov/firemap/>, January 2016). The large forest fires emit the main ozone precursors (NO_x and VOCs). Both ozone and its precursors are transported westward with the trade winds, because of that the same annual cycle can be found far away in the Atlantic Ocean (Fig. 2).

The distribution of the increasing and decreasing trends (b in Eq. 7) is indicated in Fig. 9. If the trend exceeds the $2 \times \sigma$ fit error, it is significant and the respective regions are marked with crosses.

Over central Africa and downwind over the Atlantic Ocean, a positive trend is found, and in the central equatorial Pacific a significant positive is also detected. Our results show a significant decrease over New Guinea extending to the east into the Pacific Ocean. The tropospheric ozone declines over the central America, although this trend is small and insignificant.

4.1 Seasonal trends

Besides the overall trend, the time series offers the possibility to study local or seasonal trends. The strong seasonal cycle for the TCO over the African coast is visible in Fig. 8. In this region a strong increase is found, but whether this increase is caused by increasing fire emissions or by an increase in the background TCO can hardly be explained with the figures above. In the overall trends the sine and cosine terms (Eq. 4) reflected the seasonal cycle. When focusing on the individual

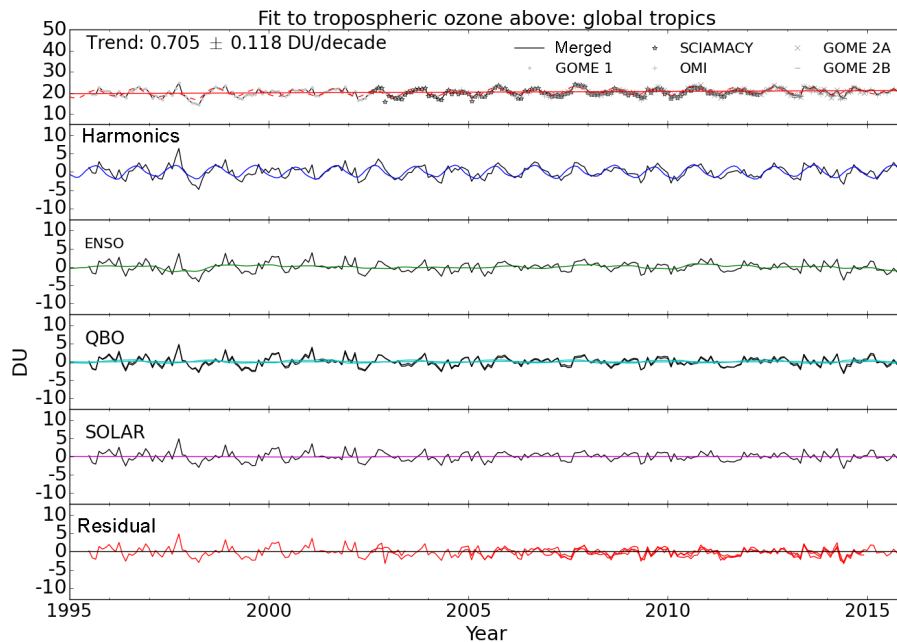


Figure 7. Fit of the tropically averaged tropospheric column ozone for the years 1995 to 2015. Top: the merged data product with the fitted linear trend is shown, the individual instruments are shown for comparison. In the next panels the harmonic functions, and the indexes for ENSO, QBO and solar activity are shown. To illustrate the instrumental variance, the bottom panel displays the residuals for the individual instruments.

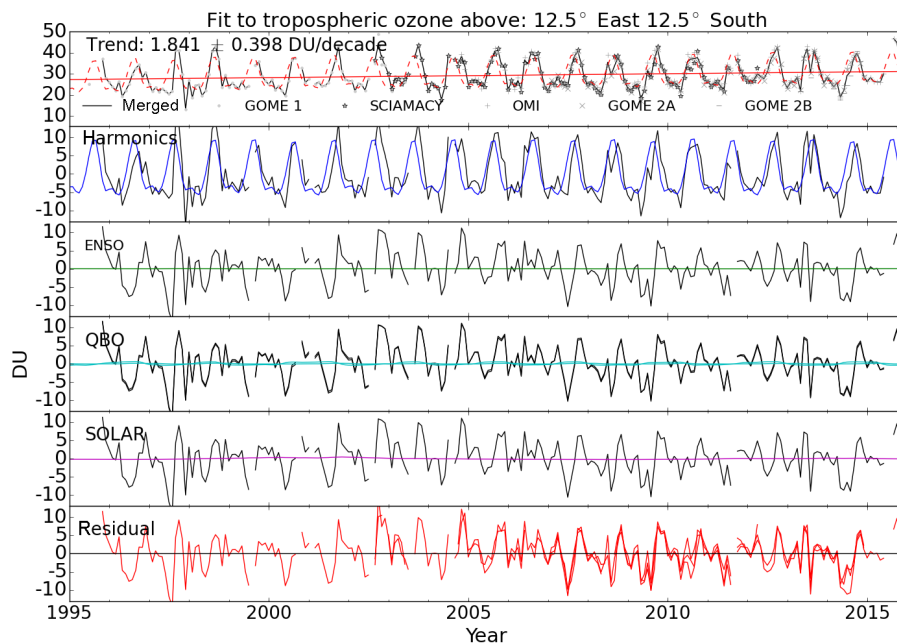


Figure 8. As Fig. 7 for the grid box showing the maximum trend. (10–15° E and 10–15° S African west coast). The time series is dominated by an annual cycle with a local ozone maximum in July/August.

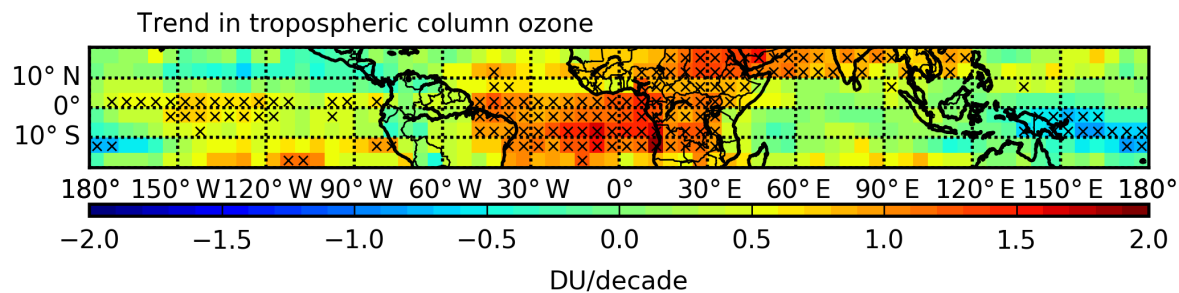


Figure 9. Tropical map of the tropospheric ozone trends. The crosses indicate regions where trends exceed the $2 \times \sigma$ fit error. Overall the tropospheric ozone increased in the last 20 years. Only for New Guinea and the neighbouring Pacific Ocean a significant decrease is found.

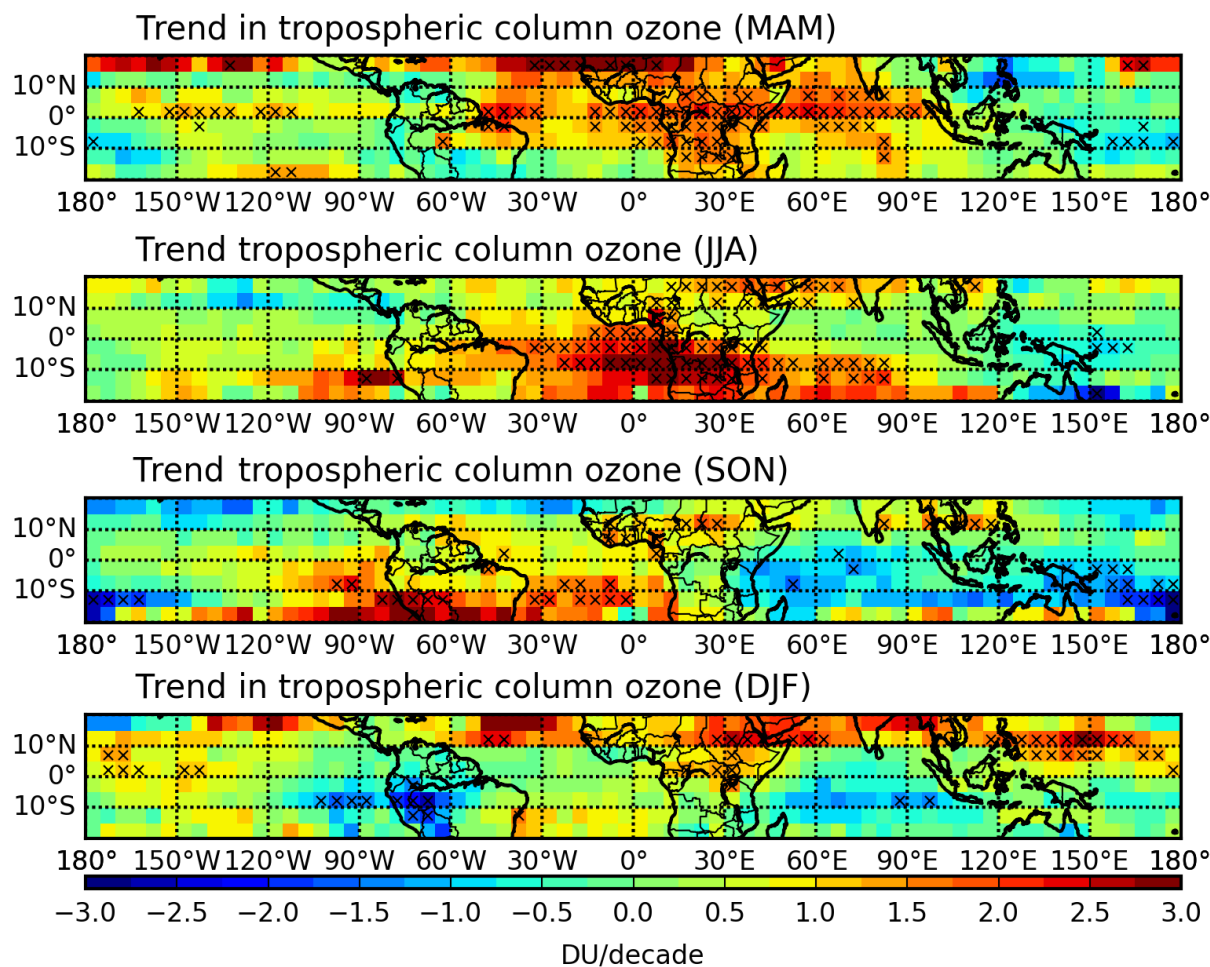


Figure 10. Same map as in Fig. 9 but for the different seasons. Note the different scale compared to Fig. 9. The main increase over southern central Africa and the Atlantic Ocean is found from June to August, which is the burning season in southern central Africa.

seasons these terms must not be considered.

$$\begin{aligned} \text{TCO}_{\text{season}} = & a + b \cdot t + e \cdot \text{ENSO}_{3.4} + f \cdot \text{solar} \\ & + g_{50} \cdot \text{QBO}_{50} + g_{30} \cdot \text{QBO}_{30} \end{aligned} \quad (8)$$

Again the fit parameters depend on the longitude and latitude, but also the trends for the tropical averages were fitted.

Maps of the seasonal trends can contribute to clarifying this question (Fig. 10). According to this figure the main increase in southern central Africa is found in the burning season, indicating that over the years more fields and forests might have been burned. Giglio et al. (2013) showed that in the pe-

riod 2000 to 2011 the burned area in Southern Hemispheric Africa increased by $1.8\% \text{ yr}^{-1}$.

For other regions like the Indian Ocean the trends have opposite signs depending on the season. The TCO decreased between September and February and increased strongly between March and May. Overall the seasonal trend maps are quite noisy compared to the general trend map. This effect might be caused by the still limited number of data ($21 \text{ years} \times 3 \text{ months} = 63$ data points in the maximum). The seasonal tropical average trends vary between $0.39 \pm 0.91 \text{ DU decade}^{-1}$ in JJA and $0.58 \pm 0.85 \text{ DU decade}^{-1}$ in SON. For all seasons the general fits are not robust and the fitted trends are less than the respective error.

5 Conclusions

Based on the GODFIT L2 ozone data from GOME, SCIAMACHY, OMI, GOME-2A and GOME-2B, we generated a harmonised data set of tropical tropospheric column ozone for the period 1995 to 2015. In the overlapping periods the TCO from the different sensors agree very well. The TCO showed an averaged increase of $0.70 \text{ DU decade}^{-1}$ or $0.35\% \text{ yr}^{-1}$.

The average tropical tropospheric ozone trend for the SCIAMACHY limb-nadir data is $\approx 0.55 \text{ DU decade}^{-1}$ or $0.2\% \text{ yr}^{-1}$ (Ebojie et. al, 2016). Cooper and Ziemke (2014) found a global (60°S to 60°N) trend of 1.9 Tg yr^{-1} ($\approx 0.7\% \text{ yr}^{-1}$ based on OMI/MLS observations). All the aforementioned trend estimates considered different time periods, the SCIAMACHY limb-nadir matching could not be applied to any of the other instruments and was only possible from 2002 to 2012. The combination of OMI and MLS data is restricted to the period after 2004. While the trend by Ebojie et. al (2016) roughly agrees with our estimate, the trend data by Cooper and Ziemke (2014) are slightly higher, though in the same order of magnitude. This might also be related to the shorter period but mainly to differences in global and tropical trend. In the year 2014 positive ozone anomalies were observed with the largest anomalies in the extratropics (Cooper and Ziemke, 2014). The positive 2014 anomaly might affect the global trend of the 10-year data set, but the largest influence will be in the extratropics where the anomaly was strongest. So for the tropics the OMI/MLS trend might be lower.

Large trends were observed over the African continent and over the Atlantic Ocean, with a maximum trend of $1.8 \text{ DU decade}^{-1}$ on the African Atlantic coast. Also Ebojie et. al (2016) and Beig and Singh (2007) observed an increase in tropospheric ozone in this region for the years 2002–2012 (4 DU decade^{-1}) and 1979–2005 ($2\% \text{ decade}^{-1} \approx 6 \text{ DU decade}^{-1}$) respectively. In both cases the respective region was smaller than in this study.

Due to the economic growth and the accompanying growing emissions, we expected a stronger positive trend in South East Asia. According to Beig and Singh (2007, in Hartmann et al., 2013) ozone columns have increased in tropical East Asia. This was partly found in the SCIAMACHY limb-nadir matching data (Ebojie et. al, 2016).

Ziemke et al. (2005) averaged TOMS CCD data for the Pacific Ocean (120°E to 120°W). They found an almost insignificant decline ($\approx 1 \text{ DU decade}^{-1}$) for 1979 to 2005 between 0 and 15°N . South of the Equator the TCO showed no trend. This partly contradicts our findings of a positive trend over large parts of the Pacific, at least for the northern part were no negative trend is found. In the south both positive and negative trends may add up to zero.

All the trend data are small ($< 1\% \text{ yr}^{-1}$) and still uncertain ($\approx 15\%$). They rely on different periods but agree on the point, that in general the tropospheric ozone in the tropics increases.

The data set will be extended as soon as new OMI, GOME-2A or GOME-2B total columns have been processed. After the launch of the Sentinel-5 Precursor mission (early 2017) also TROPOMI columns will be included. In this way the TCO data record will be extended for at least the 7-year S5P nominal mission and this will allow the monitoring of future trends in the tropical ozone. Additionally the TCO time series will be continued with the future Sentinel-5 mission. The extension will result in more reliable trend data, a temporal change in the trend might also be resolved.

6 Data availability

The harmonised TCO together with the non-harmonised TCO and the underlying GODFITv3 total column data are available on the ozone CCI web page (<http://www.esa-ozone-cci.org>, May 2016).

Acknowledgements. Financial support was given by the Bayerisches Staatsministerium für Wirtschaft und Medien, Energie und Technologie (grant 07 03/893 73/5/2013). The retrieval was developed with the grant provided in preparation for the Sentinel-5 Precursor mission. The TCO harmonisation has been performed as part of ESA's Ozone Climate Change Initiative project. We thank ESA for providing the GOME, SCIAMACHY and EUMETSAT for the GOME-2 (A and B) level 1 satellite data. We acknowledge the use of Level 1 data from Aura-OMI from NASA/KNMI. We thank the different national and international funding agencies for supporting the ozone soundings in the SHADOZ network and for providing data to the WOUDC. The World Ozone and Ultraviolet Radiation Data Centre and the SHADOZ project make the routine sonde data accessible.

The article processing charges for this open-access publication were covered by a Research Centre of the Helmholtz Association.

Edited by: J. Kim

Reviewed by: two anonymous referees

References

- Beig, G. and Singh, V.: Trends in tropical tropospheric column ozone from satellite data and MOZART model, *Geophys. Res. Lett.*, 34, L17801, doi:10.1029/2007GL030460, 2007.
- Bhartia, P.: Algorithm Theoretical Baseline Document, TOMS v8 Total ozone algorithm. available at: http://toms.gsfc.nasa.gov/version8/version8_update.html, 2003.
- Bovensmann, H., Burrows, J. P., Buchwitz, M., Frerick, J., Noel, S., Rozanov, V. V., Chance, K. V., and Goede, A. P. H.: SCIAMACHY: mission objectives and measurement modes, *J. Atmos. Sci.*, 56, 127–150, doi:10.1175/1520-0469(1999)056<0127:SMOAMM>2.0.CO;2, 1999.
- Burrows, J.P., Weber, M., Buchwitz, M., Rozanov, V. V., Ladstätter-Weißenmayer, A., Richter, A., de Beek, R., Hoogen, R., Bramstedt, K., Eichmann, K.-U., Eisinger, M., and Perner, D.: The Global Ozone Monitoring Experiment (GOME): mission concept and first scientific results, *J. Atmos. Sci.*, 56, 151–175, doi:10.1175/1520-0469(1999)056<0151:TGOME>2.0.CO;2, 1999.
- Callies, J., Corpaccioli, E., Eisinger, M., Hahne, A., and Lefebvre, A.: GOME-2 – Metop's second generation sensor for operational ozone monitoring, *ESA Bull.-Eur. Space*, 102, 28–36, available at: <http://www.esa.int/esapub/bulletin/bulletin102/Callies102.pdf>, 2000.
- Coldewey-Egbers, M., Weber, M., Lamsal, L. N., de Beek, R., Buchwitz, M., and Burrows, J. P.: Total ozone retrieval from GOME UV spectral data using the weighting function DOAS approach, *Atmos. Chem. Phys.*, 5, 1015–1025, doi:10.5194/acp-5-1015-2005, 2005.
- Coldewey-Egbers, M., Slijkhuis, S., Aberle, B., and Loyola, D.: Long-term analysis of GOME in-flight calibration parameters and instrument degradation, *Appl. Opt.*, 47, 4749–4761, doi:10.1364/AO.47.004749, 2008.
- Coldewey-Egbers, M., Loyola, D. G., Koukouli, M., Balis, D., Lambert, J.-C., Verhoelst, T., Granville, J., van Roozendael, M., Lerot, C., Spurr, R., Frith, S. M., and Zehner, C.: The GOME-type Total Ozone Essential Climate Variable (GTO-ECV) data record from the ESA Climate Change Initiative, *Atmos. Meas. Tech.*, 8, 3923–3940, doi:10.5194/amt-8-3923-2015, 2015.
- Cooper, O. R. and Zeimke, J.: Tropospheric Ozone in State of the Climate in 2014, *B. Am. Meteorol. Soc.*, 96, S48–S49, 2015.
- Cooper, O. R., Parrish, D. D., Ziemke, J., Balashov, N. V., Cupeiro, M., Galbally, I. E., Gilge, S., Horowitz, L., Jensen, N. R., Lamarque, J.-F., Naik, V., Oltmans, S. J., Schwab, J., Shindell, D. T., Thompson, A. M., Thouret, V., Wang, Y., and Zbinden, R. M.: Global distribution and trends of tropospheric ozone: An observation-based review, *Elem. Sci. Anthr.*, 2, 000029, doi:10.12952/journal.elementa.000029, 2014.
- Debaje, S. B.: Estimated crop yield losses due to surface ozone exposure and economic damage in India, *Environ. Sci. Pollut. R.*, 21, 7329–7338, doi:10.1007/s11356-014-2657-6, 2014.
- Ebojje, F., Burrows, J. P., Gebhardt, C., Ladstätter-Weißenmayer, A., von Savigny, C., Rozanov, A., Weber, M., and Bovensmann, H.: Global tropospheric ozone variations from 2003 to 2011 as seen by SCIAMACHY, *Atmos. Chem. Phys.*, 16, 417–436, doi:10.5194/acp-16-417-2016, 2016.
- Feng, Z. and Kobayashi, K.: Assessing the impacts of current and future concentrations of surface ozone on crop yield with meta-analysis, *Atmos. Environ.*, 43, 1510–1519, doi:10.1016/j.atmosenv.2008.11.033, 2009.
- Fishman, J. and Larsen, J. C.: Distribution of total ozone and stratospheric ozone in the tropics: Implications for the distribution of tropospheric ozone, *J. Geophys. Res.*, 92, 6627–6634, 1987.
- Fortuin, P. J. F. and Kelder, H.: An ozone climatology based on ozonesonde and satellite measurements, *J. Geophys. Res.*, 103, 31709–31734, doi:10.1029/1998JD200008, 1998.
- Giglio, L., Randerson, J. T., and van der Werf, G. R.: Analysis of daily, monthly, and annual burned area using the fourth-generation global fire emissions database (GFED4), *J. Geophys. Res.-Biogeo.*, 118, 317–328, doi:10.1002/jgrg.20042, 2013.
- Hartmann, D. L., Klein Tank, A. M. G., Rusticucci, M., Alexander, L. V., Brönnimann, S., Charabi, Y., Dentener, F. J., Dlugokencky, E. J., Easterling, D. R., Kaplan, A., Soden, B. J., Thorne, P. W., Wild, M., and Zhai, P. M.: IPCC 2013: Observations: Atmosphere and Surface, in: *Climate Change 2013: The Physical Science Basis. Contribution of Working Group I to the Fifth Assessment Report of the Intergovernmental Panel on Climate Change*, edited by: Stocker, T. F., Qin, D., Plattner, G.-K., Tignor, M., Allen, S. K., Boschung, J., Nauels, A., Xia, Y., Bex V., and Midgley, P. M., Cambridge University Press, Cambridge, UK, New York, NY, USA, 172–173, doi:10.1017/CBO9781107415324.008, 2013.
- Lelieveld, J., van Aardenne, J., Fischer, H., de Reus, M., Williams, J., and Winkler, P.: Increasing ozone over the Atlantic Ocean, *Science*, 304, 1483–1487, 2004.
- Lerot, C., van Roozendael, M., Spurr, R., Loyola, D., Coldewey-Egbers, M., Kochanova, S., van Gent, J., Koukouli, M., Balis, D., Lambert, J.-C., Granville, J., and Zehner, C.: Homogenized total ozone data records from the European sensors GOME/ERS-2, SCIAMACHY/Envisat and GOME-2/MetOp-A, *J. Geophys. Res.*, 119, 1639–1662, doi:10.1002/2013JD020831, 2014.
- Levelt, P. F., van den Oord, G. H. J., Dobber, M. R., Mälkki, A., Visser, H., de Vries, J., Stammes, P., Lundell, J. O. V., and Saari, H.: The ozone monitoring instrument, *IEEE T. Geosci. Remote*, 44, 1093–1101, doi:10.1109/TGRS.2006.872333, 2006.
- Leventidou, E., Eichmann, K.-U., Weber, M., and Burrows, J. P.: Tropical tropospheric ozone columns from nadir retrievals of GOME-1/ERS-2, SCIAMACHY/Envisat, and GOME-2/MetOp-A (1996–2012), *Atmos. Meas. Tech.*, 9, 3407–3427, doi:10.5194/amt-9-3407-2016, 2016.
- Loyola D., Thomas W., Spurr, R., and Mayer, B.: Global patterns in daytime cloud properties derived from GOME backscatter UV-VIS measurements, *Int. J. Remote Sens.*, 31, 4295–4318, doi:10.1080/01431160903246741, 2010.
- McPeters, R. D., Labow, G. J., and Logan, J. A.: Ozone climatological profiles for satellite retrieval algorithms, *J. Geophys. Res.*, 112, D05308, doi:10.1029/2005JD006823, 2007.

- Miles, G. M., Siddans, R., Kerridge, B. J., Latter, B. G., and Richards, N. A. D.: Tropospheric ozone and ozone profiles retrieved from GOME-2 and their validation, *Atmos. Meas. Tech.*, 8, 385–398, doi:10.5194/amt-8-385-2015, 2015.
- Monks, P. S., Archibald, A. T., Colette, A., Cooper, O., Coyle, M., Derwent, R., Fowler, D., Granier, C., Law, K. S., Mills, G. E., Stevenson, D. S., Tarasova, O., Thouret, V., von Schneidemesser, E., Sommariva, R., Wild, O., and Williams, M. L.: Tropospheric ozone and its precursors from the urban to the global scale from air quality to short-lived climate forcer, *Atmos. Chem. Phys.*, 15, 8889–8973, doi:10.5194/acp-15-8889-2015, 2015.
- Nawrot, T., Nemmar, A., and Nemery, B.: Update in Environmental and Occupational Medicine 2005, *Am. J. Resp. Crit. Care*, 173, 948–952, doi:10.1164/rccm.2601010, 2006.
- Oltmans, S. J., Lefohn, A. S., Shadwick, D., Harris, J. M., Scheel, H. E., Galbally, I., Tarasick, D. W., Johnson, B. H., Brunke, E.-G., Claude, H., Zeng, G., Nichol, S., Schmidlin, F., Davies, J., Cuevas, E., Redondas, A., Naoe, H., Nakano, T., and Kawasato, T.: Recent tropospheric ozone changes – A pattern dominated by slow or no growth, *Atmos. Environ.*, 67, 331–351, doi:10.1016/j.atmosenv.2012.10.057, 2013.
- Parrish, D. D., Lamarque, J.-F., Naik, V., Horowitz, L., Shindell, D. T., Staehelin, J., Derwent, R., Cooper, O. R., Tanimoto, H., Volz-Thomas, A., Gilge, S., Scheel, H.-E., Steinbacher, M., and Fröhlich, M.: Long-term changes in lower tropospheric baseline ozone concentrations: Comparing chemistry-climate models and observations at northern mid-latitudes, *J. Geophys. Res.-Atmos.*, 119, 5719–5736, doi:10.1002/2013JD021435, 2014.
- Saunois, M., Emmons, L., Lamarque, J.-F., Tilmes, S., Wespes, C., Thouret, V., and Schultz, M.: Impact of sampling frequency in the analysis of tropospheric ozone observations, *Atmos. Chem. Phys.*, 12, 6757–6773, doi:10.5194/acp-12-6757-2012, 2012.
- Schuessler, O., Loyola, D., Doicu, A., and Spurr, G.: Information Content in the Oxygen A-band for the Retrieval of Macrophysical Cloud Parameters, *IEEE T. Geosci. Remote*, 52, 3246–3255, doi:10.1109/TGRS.2013.2271986, 2014.
- Sprenger, M., Croci Maspoli, M., and Wernli, H.: Tropopause folds and cross-tropopause exchange: A global investigation based upon ECMWF analyses for the time period March 2000 to February 2001, *J. Geophys. Res.*, 108, 8518, doi:10.1029/2002JD002587, 2003.
- Spurr, R., Natraj, V., Lerot, C., van Roozendael, M., and Loyola D.: Linearization of the Principal Component Analysis method for radiative transfer acceleration: Application to retrieval algorithms and sensitivity studies, *J. Quant. Spectrosc. Ra.*, 125, 1–17, doi:10.1016/j.jqsrt.2013.04.002, 2013.
- Sun, L., Xue, L., Wang, T., Gao, J., Ding, A., Cooper, O. R., Lin, M., Xu, P., Wang, Z., Wang, X., Wen, L., Zhu, Y., Chen, T., Yang, L., Wang, Y., Chen, J., and Wang, W.: Significant increase of summertime ozone at Mount Tai in Central Eastern China, *Atmos. Chem. Phys.*, 16, 10637–10650, doi:10.5194/acp-16-10637-2016, 2016.
- Thompson, A. M., Witte, J. C., McPeters, R. D., Oltmans, S. J., Schmidlin, F. J., Logan, J. A., Fujiwara, M., Kirchhoff, V. W. J. H., Posny, F., Coetzee, G. J. R., Hoegger, B., Kawakami, S., Ogawa, T., Johnson, B. J., Vömel, H., and Labow, G.: Southern Hemisphere Additional Ozonesondes (SHADOZ) 1998–2000 tropical ozone climatology 1. Comparison with Total Ozone Mapping Spectrometer (TOMS) and ground-based measurements, *J. Geophys. Res.*, 108, 8238, doi:10.1029/2001JD000967, 2003.
- Valks, P. J. M., Koelemeijer, R. B. A., van Weele, M., van Velthoven, P., Fortuin, J. P. F., and Kelder, H.: Variability in tropical tropospheric ozone: Analysis with Global Ozone Monitoring Experiment observations and a global model, *J. Geophys. Res.*, 108, 4328, doi:10.1029/2002JD002894, 2003.
- Valks, P., Hao, N., Gimeno Garcia, S., Loyola, D., Dameris, M., Jöckel, P., and Delcloo, A.: Tropical tropospheric ozone column retrieval for GOME-2, *Atmos. Meas. Tech.*, 7, 2513–2530, doi:10.5194/amt-7-2513-2014, 2014.
- van Roozendael, M., Spurr, R., Loyola, D., Lerot, C., Balis, D., Lambert, J.-C., Zimmer, W., van Gent, J., van Geffen, J., Koukouli, M., Granville, J., Doicu, A., Fayt C., and Zehner C.: Sixteen years of GOME/ERS-2 total ozone data: The new direct-fitting GOME Data Processor (GDP) version 5 Algorithm description, *J. Geophys. Res.*, 117, D03305, doi:10.1029/2011JD016471, 2012.
- Wang, P., Stammes, P., van der A, R., Pinardi, G., and van Roozendael, M.: FRESCO+: an improved O₂ A-band cloud retrieval algorithm for tropospheric trace gas retrievals, *Atmos. Chem. Phys.*, 8, 6565–6576, doi:10.5194/acp-8-6565-2008, 2008.
- Young, P. J., Archibald, A. T., Bowman, K. W., Lamarque, J.-F., Naik, V., Stevenson, D. S., Tilmes, S., Voulgarakis, A., Wild, O., Bergmann, D., Cameron-Smith, P., Cionni, I., Collins, W. J., Dal-søren, S. B., Doherty, R. M., Eyring, V., Faluvegi, G., Horowitz, L. W., Josse, B., Lee, Y. H., MacKenzie, I. A., Nagashima, T., Plummer, D. A., Righi, M., Rumbold, S. T., Skeie, R. B., Shindell, D. T., Strode, S. A., Sudo, K., Szopa, S., and Zeng, G.: Pre-industrial to end 21st century projections of tropospheric ozone from the Atmospheric Chemistry and Climate Model Intercomparison Project (ACCMIP), *Atmos. Chem. Phys.*, 13, 2063–2090, doi:10.5194/acp-13-2063-2013, 2013.
- Ziemke, J. R., Chandra, S., and Bhartia, P. K.: Two new methods for deriving tropospheric column ozone from TOMS measurements: The assimilated UARS MLS/HALOE and convective-cloud differential techniques, *J. Geophys. Res.*, 103, 22115–22127, 1998.
- Ziemke, J. R., Chandra, S., and Bhartia, P. K.: A 25-year data record of atmospheric ozone from TOMS Cloud Slicing: Implications for trends in stratospheric and tropospheric ozone, *J. Geophys. Res.*, 110, D15105, doi:10.1029/2004JD005687, 2005.
- Ziemke, J. R., Joiner, J., Chandra, S., Bhartia, P. K., Vasilkov, A., Haffner, D. P., Yang, K., Schoeberl, M. R., Froidevaux, L., and Levelt, P. F.: Ozone mixing ratios inside tropical deep convective clouds from OMI satellite measurements, *Atmos. Chem. Phys.*, 9, 573–583, doi:10.5194/acp-9-573-2009, 2009.
- Ziemke, J. R., Chandra, S., Labow, G. J., Bhartia, P. K., Froidevaux, L., and Witte, J. C.: A global climatology of tropospheric and stratospheric ozone derived from Aura OMI and MLS measurements, *Atmos. Chem. Phys.*, 11, 9237–9251, doi:10.5194/acp-11-9237-2011, 2011.
- Ziemke, J. R. and Chandra, S.: Development of a climate record of tropospheric and stratospheric column ozone from satellite remote sensing: evidence of an early recovery of global stratospheric ozone, *Atmos. Chem. Phys.*, 12, 5737–5753, doi:10.5194/acp-12-5737-2012, 2012.